Scanning Capacitance Microscopy Investigations of Focused Ion Beam Damage in Silicon

W. Brezna, H. Wanzenböck, A. Lugstein, E. Bertagnolli, E. Gornik, J. Smoliner

Institute for Solid State Electronics, Vienna University of Technology

In this article, we explore the application of Scanning Capacitance Microscopy (SCM) for studying focused ion beam (FIB) induced damage in silicon. We qualitatively determine the technologically important beam shape by measuring the SCM image of FIB processed implantation spots and by comparison of topographical and SCM data. Further, we investigate the question how deep impinging ions generate measurable damage below the silicon surface. For this purpose, trenches were manufactured using FIB and analyzed by SCM in cross sectional geometry.

Introduction

Focused ion beam (FIB) techniques are among the most important tools for modification tasks below 100 nanometer. Today, FIB systems are mainly used for device modification, transmission electron microscopy (TEM) sample preparation, scanning probe microscopy (SPM) tip preparation, and deposition of different metals and insulators [1]. Unfortunately, there are mainly two effects that limit the usage of FIB modification to certain applications and areal scales [2]. Difficult to measure, the ion beam diameter and intensity profile defines the lateral resolution and the smallest possible size of a FIB made structure. The other limitation occurs due to ion beam induced damage, which extends far below the modified sample surface.

Various methods such as secondary ion mass spectroscopy (SIMS) and transmission electron microscopy (TEM) have been utilized to measure penetration depths and intensity profiles of FIBs. However, the disadvantage of these methods is their lack of 2D spatial resolution (SIMS) or difficult sample preparation (TEM). For this reason, scanning probe techniques have successfully been applied for FIB intensity profile determination and imaging in other ion beam applications [3]. Topographic atomic force microscopy (AFM) investigations can yield high resolution data from FIB implanted spots via the embossment of FIB amorphisized areas due to the slightly lower density of amorphous silicon compared to crystalline silicon. However, severe degradation of the electronic properties will occur long before the structural changes (amorphization) take place, which cannot be investigated any more with topographic AFM. In this article, we introduce Scanning Capacitance Microscopy (SCM) as a very sensitive tool to investigate the position and extent of FIB induced electronic degradation. SCM is an extension of conventional AFM and a very promising tool for semiconductor device characterization. The current state of the art of this technique can be found in the review article [4]. SCM can detect magnitudes smaller changes in material composition than any other scanning probe method and it is possible to sense as small quantities as 10 – 100 impurity atoms per cubic micron (10^{13} – 10^{14} per cm^3). Where FIB irradiation does not alter the topography of the region of interest, it is still possible to get reliable data of the FIB damaged areas via SCM. We first use this method to determine the ion beam intensity profile by investigating irradiated silicon surfaces. Then we will deal with the damage spread inside the silicon sample beneath a FIB milled trench.

Experimental

To avoid any additional difficulties in data interpretation due to the very complex electrical behavior of pn-junctions [5] we decided to use low p-doped silicon wafers, since our FIB system is equipped with a Ga^+ ion source (acceptors). The low acceptor concentration of the bulk material was an advantage, because SCM yields higher signals on low-doped semiconductors. The samples were prepared in two ways to match the different demands of FIB intensity profile and damage depth determination: For measuring the beam intensity profile, we used the very clean surfaces of freshly cleaved silicon wafers. On the cleaved surface five types of spots were made with the FIB system, which differed from each other in the deposited ion dose (0.025, 0.05, 0.1, 0.5 and 5 pC/spot). The spots were located in close vicinity (a few microns) of the wafer edge to reduce sample tip-holder overlaps and related stray capacitance, which increases the signal to noise ratio in our SCM measurements. The acceleration voltage of the Ga^+ ions was 50 kV and the aperture size was 50 µm. For the investigation of the damage depths, a trench was milled into the polished front side of a wafer. After milling, the sample was cleaved to get cross sections of the damaged area beneath the trench.

Results and Discussion

Although the SCM signal is a complicated function of the semiconductor doping concentration and the applied tip-bias voltage, it is possible to adjust the electrical parameters of the setup in a way to gain a signal that is monotonic with doping concentration [6]. Using such optimized conditions leads to good SCM contrast with big signal in low-doped regions and small signal in higher doped regions. However, besides the p-type doping by Ga^+ ion implantation, the crystalline structure of FIB irradiated samples is damaged heavily which also results in a reduction of the SCM signal. Therefore, we cannot distinguish between high doped or damaged areas. Studies show that ion beam doses magnitudes smaller than the minimum dose for surface modification (e.g. swelling due to amorphization) can already be detected via SCM. We used this fact to determine the beam intensity profile of our FIB system. Figure 1 (a) shows the resulting topographic changes of milling with a moderate dose per spot (0.5 pC/spot). The swelling and subsequent silicon removal due to sputtering can be seen very well and leads to the typical crater-like structures. Figure 1 (b) shows the simultaneously measured SCM picture. In comparison with the topographic image seen in Fig. 1 (a), the recorded SCM picture shows a significantly larger damaged region indicated by the dark circle of low SCM signal. Based on topography, we define the ion beam radius as follows: the radius R_{Topo} is the distance from the deepest milled point (highest intensity in the beam center) to the point where the outer swelling flank is half-decayed. In the case where the ion dose is so small that only swelling is observed, we take the distance between the maximum of the swelling and the point where it is half-decayed. Based on SCM we defined the beam radius R_{SCM} as half the distance between the points where the SCM-signal-flanks rise to half of their maximum.

The two radii R_{Topo} and R_{SCM} are compared in Fig. 1 (c), where cross sections of the image data are plotted along line L. The difference between topography signal and SCM signal, $\Delta R = R_{SCM} - R_{Topo}$, is 250 nm. Figure 1 (d) compares the behavior of the radii R_{Topo} and R_{SCM} with increasing dose per spot. The radii show monotonic growth, however, there are saturation effects in the high dose regime. In addition, both data sets diverge for big ion doses. Whereas for the lowest dose the structures have twice the radius in SCM mode than in topography mode, for the highest dose this ratio is almost four. Our observation that the SCM based beam radius R_{SCM} is always larger than the topographic radius R_{Topo}, and the effect that R_{Topo} and R_{SCM} diverge for big ion doses, can be explained by the following facts. First, as was already published [1], [7], the beam profile consists of (at least) two regions: The region far away from the beam

center, where the overall intensity is very small but decays slowly. The other region is close to the beam center, where the intensity is comparable with the beam center and has the steepest decay. Second, SCM is much more sensitive to ion irradiation effects than the topographic signal, since topographic changes by amorphization need very high ion doses. Because of these two properties, the SCM sensed radius grows quickly with increasing dose per spot in the outer areas of the beam profile, whereas the smaller crater-like structure in the topography grows just slowly.

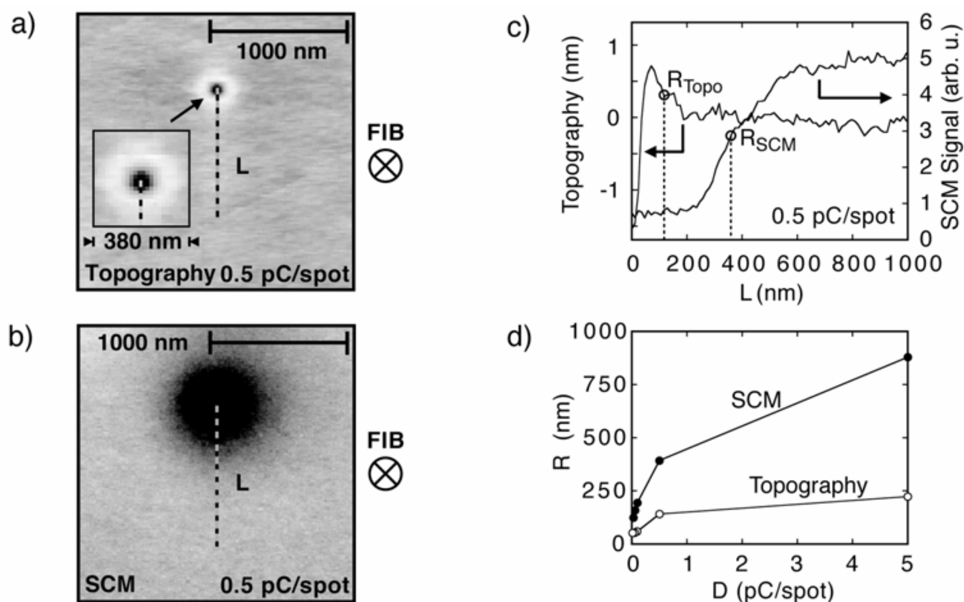

Fig. 1: (a) The topographic image of a FIB irradiated spot with an inset showing a magnification. The beam direction is indicated. (b) Corresponding SCM image. (c) Radial cross sections through the topographic and SCM images along the line L. R_{Topo} and R_{SCM} define the radius of damage as seen in the topographic and the SCM image. (d) R_{Topo} and R_{SCM} versus ion dose D.

A second important subject for FIB application is the determination of the width and depth of FIB induced damage below the sample surface. Figure 2 (a) shows the topography of the cleaved, FIB made trench. The corresponding SCM signal is shown in Fig. 2 (b). Again, we optimized the SCM bias to obtain the largest SCM signals in the unimplanted, low-doped areas. Figure 2 (c) compares the topographic and the SCM signal height plotted along line $L_{||}$ parallel to the incident beam. The distance between the trenches side walls and the SCM signal $\Delta R_{||}$ is approximately 620 nm. Previous TEM investigations of deep FIB milled polysilicon show an amorphisized region that extends about 200 nm in depth [8], which is only a third of the distance we have measured.

This can be explained by comparing the detection sensitivity of TEM and SCM. To get contrast in TEM, a crystalline substrate has to be amorphizised to a high extent, which needs relatively high ion doses. On the other hand, SCM is able to detect impurity concentrations down to 10 – 100 atoms per μm^3 (10^{13} - 10^{14} per cm^3), which is magnitudes more sensitive than TEM. Figure 2 (d) shows plots of the topographic and the SCM signal heights along line L perpendicular to the FIB direction. With a certain probability, ions can be scattered out of their incident direction. In this way, they can reach areas not covered by the beam area. The distance between the trenches sidewall and the SCM signal $\Delta R_{\perp}$ is about 310 nm. A comparison between Fig. 2 (d) and Fig. 2 (c) shows a ratio $\Delta R_{\perp}/\Delta R_{||}$ of 1/2, which is confirmed by previous TEM investigations of FIB induced damage in polysilicon-gates of MOSFETs [8].

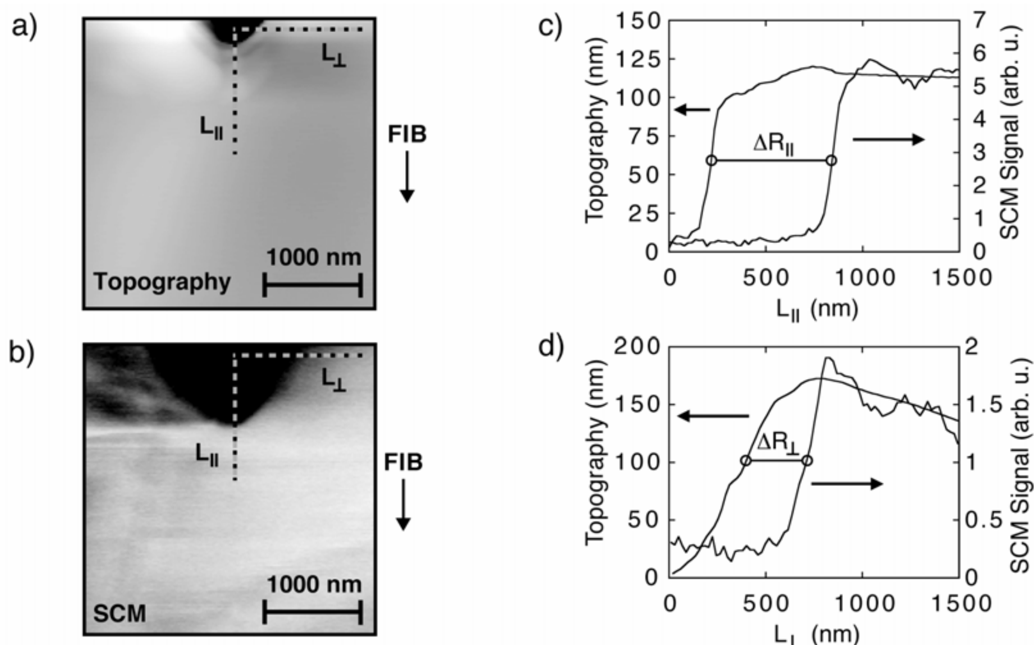

Fig. 2: (a) The topographic image of a FIB milled trench in cross sectional view. The beam direction is indicated. (b) Simultaneously recorded SCM image. (c) Comparison of topographic and SCM signal heights along the line $L_{||}$ parallel to the ion beam. (d) Topographic and SCM signal heights along the line $L_{\perp}$ perpendicular to the incident beam.

Conclusion

In summary, we demonstrated the utilization of SCM for the characterization of FIB processed samples. First, the beam shape of a FIB machine was determined by taking SCM images of spots created by FIB irradiation. Our data indicate a beam shape consisting of a high intensity central region, which decays very quickly when the center is left, and vast tails where the intensity is small but declines more slowly with radial distance. Second, we investigated how deep below the FIB modified surface changes in the structural and electrical properties can be sensed. Damage was detected in much greater depths than reported by other authors, which is probably due to the increased sensitivity of SCM compared to other methods. Finally, the damage depth in the direction parallel to the incident beam and perpendicular to it has been investigated and was found to be in agreement with literature.

Acknowledgements

This work was sponsored by “Fonds für innovative Projekte an der TU Wien”, “Gesellschaft für Mikroelektronik (GMe)” and “Fonds zur Förderung der wissenschaftlichen Forschung (FWF)” project No Z24-TPH.

References

[1] J. Melngailis, J. Vac. Sci. Technol. B5, 469 (1987)

[2] C. Lehrer, L. Frey, S. Petersen, H. Ryssel; J. Vac. Sci. Technol. B19, 2533 (2001)

[3] T. Winzell, S. Anand, I. Maximov, E. L. Sarwe, M. Graczyk, L. Montelius, H. J. Whitlow; Nucl. Instrum. Methods B173, 447 (2001)

[4] D. D. Bugg, P. J. King; J. Phys. E21, 147 (1988)

[5] M. L. O'Malley, G. L. Timp, S. V. Moccio, J. P. Garno, R. N. Kleiman; Appl. Phys. Lett. 74, 272 (1999)

[6] J. Smoliner, B. Basnar, S. Golka, E.Gornik, B.Löffler, M.Schatzmayr, H. Enichlmair; Appl. Phys. Lett. 79, 3182 (2001)

[7] P. D. Rose, S. J. Brown, G. A. C. Jones, D. A. Ritchie; Microelectronic Engineering 41/42, 229 (1998)

[8] A. Lugstein, W. Brezna, E. Bertagnolli; IEEE Internat. Reliability Phys. Symp. IRPS proceedings, 369 (2002)